Exciton Scattering on Symmetric Branching Centers in Conjugated Molecules

Hao Li,[†] Chao Wu,[‡] Sergey V. Malinin,[†] Sergei Tretiak,*[§] and Vladimir Y. Chernyak*[†]

[†]Department of Chemistry, Wayne State University, 5101 Cass Avenue, Detroit, Michigan 48202, United States

[‡]Department of Chemical and Biomolecular Engineering, University of Notre Dame, 182 Fitzpatrick Hall, Notre Dame, Indiana 46556, United States

[§]Theoretical Division, Center for Nonlinear Studies, and Center for Integrated Nanotechnologies, Los Alamos National Laboratory, Los Alamos, New Mexico 87545, United States

ABSTRACT: The capability of the exciton scattering approach, an efficient methodology for excited states in branched conjugated molecules, is extended to include symmetric triple and quadruple joints that connect linear segments on the basis of the phenylacetylene backbone. The obtained scattering matrices that characterize these vertices are used in application of our approach to several test structures, where we find excellent agreement with the transition energies computed by the reference quantum chemistry. We introduce topological charges, associated with the scattering matrices, which help to formulate useful relations

$L = 2$: 2 excitations in the band

$L = 7$: 6 excitations in the band and 1 bound state above the band

between the number of excitations in the exciton band and the number of repeat units. The obtained features of the scattering phases are analyzed in terms of the observed excited state electronic structure.
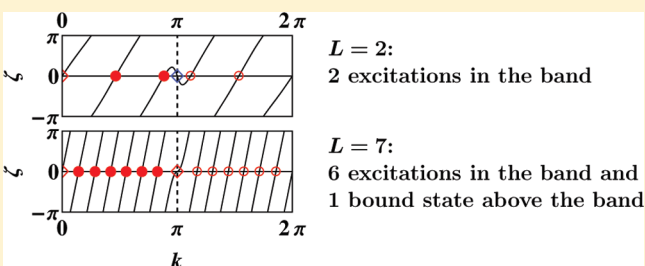
I. INTRODUCTION

Carbon-rich molecular structures may exhibit remarkable electronic and optical properties[1−11] due to the high degree of π-conjugation, strong electron—electron correlations, and electron—phonon coupling. Such conjugated molecules can be used in a variety of optical and photovoltaic applications.[12−21] However, these complex systems are very hard to study theoretically with both satisfactory efficiency and accuracy, especially when the properties involve excited electronic states. The latter typically correspond to tightly bound excitons due to low-dimensionality and a low dielectric constant in these materials. Consequently, correct description of such excited states should include a large amount of electronic correlations (many-body effects).[22−28] Moreover, strong electron—phonon coupling and substantial conformational disorder[29−31] also significantly complicate theoretical modeling and interpretation of spectroscopic experiments.

In the mid-1990s, Mukamel and co-workers developed a collective electronic oscillator (CEO) picture of electronic excitations in conjugated systems and semiconductors in which electronic excitations are associated with collective electronic modes, characterized by the matrix elements of the single-electron density matrix operator between the ground and the relevant excited state, and visualized using 2D color contour plots (see, for example, refs 32, 33, and 34 for a comprehensive review). With the emphasis on the size-scaling properties of the off-resonant as well as resonant optical response in conjugated polymers, these studies were focused on the long-wave excitations and addressed the interpretation of their properties

mostly in terms of the relative motion of electrons and holes. The off-diagonal size of a mode in long enough oligomers represents an important coherence size which allows of a simple and intuitive interpretation of the optical response in conjugated systems and its scaling properties. Applications include analysis of linear and nonlinear optical properties of conjugated molecules; in particular, size-scaling and saturation of second-order polarizability in long donor/acceptor substituted polyens[35] and localization of optical excitations in meta-substituted phenylacetylene dendrimers.[36]

The importance of the exciton "center-of-mass" motion was realized much later in the context of electron energy loss spectroscopy that allows direct observation of the transition charge spatial distributions, associated with short-wave electronic excitations, by measuring the dynamic structure factor.[37,38] It was demonstrated that the relevant signals can be interpreted in terms of the center-of-mass exciton motion, rather than the relative electron—hole motion and, more specifically, by treating an excitation as an exciton particle in a box. The oscillating patterns of the collective electronic modes in the diagonal direction that reflects quantization of the center-of-mass motion were also reported in ref 39.

The idea of applying the particle in a box concept to handle electronic excitations in conjugated systems with more complicated geometry (e.g., dendrimers (tree-like branched molecules) or more general branched structures that contain loops) was first discussed in ref 40. There we demonstrated on a qualitative level that one can get an adequate picture of optical excitations in branched conjugated molecules (including the excitation energies and the oscillator strengths) if the excitations are represented as standing waves on the linear segments formed by scattering at the molecular vertices (branching centers, joints, and chain termini).

The exciton scattering (ES) approach to excited state electronic structure in conjugated systems was first formulated in ref 41, where we also demonstrated its capability not only to make qualitative predictions but also to provide accurate quantitative results for the excitation energies. In the following series of publications,[42−45] we developed the ES approach for excited state electronic structure of branched conjugated molecules. The ES approach is based on mapping the original problem onto a much simpler and computationally inexpensive problem of finding the eigenstates of a quantum particle on the corresponding graph, whose edges and vertices represent the linear segments and molecular vertices of the considered molecule. The ES approach was put on a firm theoretical basis[42] as an approximation that becomes asymptotically exact in the limit when the linear segments are much longer than the exciton size. Within the ES approach, the excited state energies (more precisely, the transition energies with respect to the ground state) are determined by solving a $2N \times 2N$ generalized linear spectral problem, with N being the number of linear segments in the underlying conjugated molecule. The input for the ES equations is represented by the ES parameters: the exciton dispersion $\omega(k)$ that relates the transition energy ω to the exciton center-of-mass momentum k in an infinitely long polymer, as well as the ω-dependent $n \times n$ scattering matrices $\Gamma(\omega)$ associated with the vertices (termini, double joints, and branching centers correspond to $n = 1$, $n = 2$, and $n \geq 3$, respectively).

In refs 41 and 43, we developed a strategy for retrieving first the exciton dispersion together with the scattering amplitude at the molecular termini and, next, the 2×2 scattering matrices for double joints from quantum-chemical calculations in relevant molecular fragments of moderate size. This strategy was implemented for both the time-dependent density functional[41] and time-dependent Hartree−Fock[43] methods using an example of phenylacetylene (PA, or poly phenylene ethynylene, PPE) systems[7,8] including unmodified chain termini, as well as ortho and meta joints. We further benchmarked the ES approach by comparing the excitation energies obtained via solving the ES equations, using the retrieved ES parameters, with the quantum-chemical calculations in a variety of test molecules. For all PA-based molecules studied thus far, the ES approach produced impressively accurate results.[41,44] The ES method was extended to calculations of the transition dipoles,[45] for which it showed sufficiently high accuracy with respect to the reference quantum chemistry computations. Very recently, we have used the ES method to describe the donor and acceptor substitutions and obtained the exciton scattering amplitudes at the modified termini.[46]

In this paper, we extend the capability of the ES approach by retrieving the 3×3 and 4×4 frequency-dependent scattering matrices that describe symmetric triple and quadruple joints, referred to as Y and X joints, respectively. This allows us to extend the ES methodology to a much broader variety of branched conjugated molecules and molecular networks that consist of the characterized building blocks. We also present initial studies of the analytical properties of the scattering matrices $\Gamma(\omega)$ and, in particular, relate some simple topological invariants, associated with $\Gamma(\omega)$ to the number of electronic excitations in the conjugated molecules that contain the corresponding joints.

The manuscript is organized as follows: In Section II, we review the ES approach. Then we focus on two symmetric higher-order joints: the Y- (symmetric triple, all-meta) joint and the X-(symmetric quadruple) joint. We extract their scattering matrices by taking advantage of their symmetry (Section III). The knowledge of the two additional scattering matrices allows us to explore a much wider variety of molecular structures represented by any combination of the molecular building blocks that have been characterized before. Results for the transition energies obtained within the ES approach are analyzed for several test molecules in Section IV. Finally, general topological properties of the scattering phases of the vertices of conjugated polymeric structures are discussed in Section V.

II. REVIEW OF THE ES APPROACH

A. Exciton Scattering Formalism. The ES approach was introduced in refs 40 and 41 and later described in some more detail in refs 42 and 45. For the sake of self-sufficiency of this manuscript, in this subsection, we present a brief overview of the ES formalism.

Within the ES approach, an excitation in a conjugated molecule is associated with a state of a quantum particle (exciton[17,22,26,47,48]) on the corresponding graph. In a perfect, infinite, linear polymer, an exciton with a quasimomentum k corresponds to an excitation with a certain energy ω. Thus, excitons are described by a dispersion relation $\omega(k)$ between the center-of-mass quasimomentum (wavenumber) and the energy. Due to the discrete nature of translational symmetry (we use integers to label the repeat units), exciton quasimomenta k reside in a 1D Brillouin zone $0 \leq k \leq 2\pi$. Molecular vertices violate the discrete translational symmetry of the perfect polymer and mix waves with opposite wavenumbers. Far from the molecular vertices, the exciton wave function is a superposition of two plane waves, e^{ikx} and e^{-ikx}. For the clarity of the analogy between the electronic excitation of a molecule and the quantum particle (exciton), we have to tolerate a slight complication of the ES formalism: the exciton wave function should be related to the distribution of transition dipoles and, hence, possesses properties of a vector. Since the transition dipole of a linear segment is directed along the backbone, the exciton wave function on segment α can be represented (within the ES formalism) as a vector function,

$$\boldsymbol{\psi}_\alpha(x) = \boldsymbol{\sigma}_\alpha \, \psi_\alpha(x; \boldsymbol{\sigma}_\alpha), \quad \psi_\alpha(x; -\boldsymbol{\sigma}_\alpha) = -\psi_\alpha(x; \boldsymbol{\sigma}_\alpha) \quad (1)$$

expressed in terms of the orientation-dependent scalar function $\psi_\alpha(x; \boldsymbol{\sigma}_\alpha)$, where $\boldsymbol{\sigma}_\alpha$ is a unit vector along segment α, defined up to a sign factor. It is clear from eq 1 that the vector character of the segment exciton wave function can be interpreted as follows: The projection of the exciton wave function on an edge is defined with respect to a choice of the edge orientation; the sign of the projection is changed when the edge orientation is reversed. It is worth noting that, due to the dipole-distribution interpretation of the exciton wave function within the ES approach, $\psi(x; \boldsymbol{\sigma})$ in a

5466

dx.doi.org/10.1021/jp110317d |*J. Phys. Chem. B* 2011, 115, 5465–5475

linear oligomer is symmetric for the first (bright) excitation and antisymmetric for the second (dark) excitation, etc.

Within the ES approach, the exciton wave function can be found by solving standard (apart from the vector features) wave equations on a graph that describe exciton propagation along its edges and scattering at its vertices. We refer to these equations as ES equations and formulate them in terms of the incoming ($-$) and outgoing ($+$) waves $\psi_{\alpha b}^{(\mp)}$, defined as the values of the respective (incoming/outgoing) components of the wave function on segment α at vertex b. The first subset of equations accounts for the exciton propagation along the linear segments. For a segment α of length L_α between the vertices b and c, we have

$$\psi_{\alpha b}^{(-)} = n_{b\alpha}\left(n_{c\alpha} \cdot \psi_{\alpha c}^{(+)}\right) \exp(ikL_\alpha) \qquad (2)$$

where $n_{v\alpha}$ is a unit vector at vertex v along the edge α, naturally defined up to sign factor that can be specified in an arbitrary way. The second subset of wave equations on a graph describe scattering at the vertices. For a vertex b characterized by an energy-dependent scattering matrix $\Gamma_b(\omega)$, we have

$$\psi_{\alpha b}^{(+)} = n_{b\alpha} \sum_{\beta \ni b} \Gamma_{b,\alpha\beta}(\omega; n_b)\left(n_{b\beta} \cdot \psi_{\beta b}^{(-)}\right) \qquad (3)$$

where n_b denotes a set of vectors $n_{b\alpha}$ with α running over all adjacent edges, and changing the sign of $n_{b\alpha}$ should be accompanied by the change of sign for the matrix elements $\Gamma_{b,\alpha\beta}$ and $\Gamma_{b,\beta\alpha}$ for $\beta \neq \alpha$ with the rest of the matrix elements remaining unchanged.

At this point, we emphasize that a particular choice of the directions (signs) of the vectors σ_α and $n_{b\alpha}$ turns eq 2 together with eq 3 into a system of scalar equations for $\psi_{\alpha b}^{\pm}$. Changing the signs of any combination of σ_α and $n_{b\alpha}$ turns these equations into a system of equivalent equations. This can be interpreted as *gauge* invariance of the above system of equations, whereas a choice of a particular orientation for σ_α and $n_{b\alpha}$ should be referred to as gauge fixing.

The scattering matrix of a vertex of degree n (i.e., n segments are connected to it) is an $n \times n$ unitary symmetric matrix, with the latter feature due to time-reversal symmetry.[43] For the sake of the presentation simplicity and clarity, we restrict our general formalism to a single exciton type (in terms of the electron–hole relative motion), which makes one dispersion relation and a single set of scattering matrices sufficient for description of all excitations.

Provided the exciton dispersion $\omega(k)$ and the energy-dependent scattering matrices $\Gamma(\omega)$ for all vertices are known, the excitation energies and wave functions (up to a normalization factor) can be found by solving a homogeneous system of ω-dependent linear equations (a generalized spectral problem), represented by eq 2 combined with eq 3. Thus, the concept of a library of molecular building blocks, addressed in the next subsection, becomes an important ingredient of the ES methodology.

B. Library of Molecular Building Blocks. A branched conjugated molecule consists of two types of structural units: linear segments and molecular vertices. The vertices and the repeat units comprising the linear segments are molecular building blocks. The exciton dispersion relation $\omega(k)$ characterizes the property of the repeat unit and a particular exciton type. Therefore, instead of quantum-chemical computations in large conjugated molecules with partial translational symmetry, within the
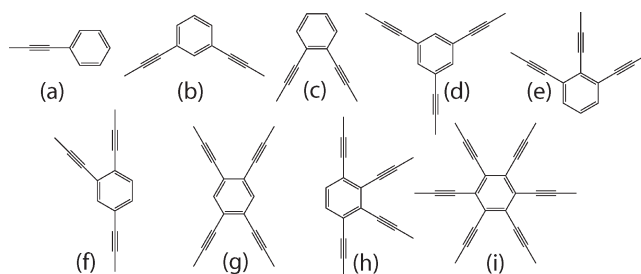
Figure 1. Possible phenylacetylene (PA) vertices.

ES approach, one uses this single dispersion relation, which can be obtained from computations in relatively short linear molecules. Similarly, in a large conjugated system, there are usually only a few different vertex types. Therefore, a single scattering matrix can characterize a large number of vertices of the corresponding type, which further improves numerical efficiency of the ES approach. In addition to the exciton dispersion and scattering matrices, the ES parameters include the ω-dependent transition charges and dipole parameters that determine how the contributions to the total transition dipole, associated with individual building blocks of a particular type, depend on the local excitation amplitude.[45]

All ES parameters of molecular building blocks can be tabulated, systematized, and collected in a library of molecular building blocks for a specific quantum-chemical method. One can use the most adequate quantum-chemical method for the particular system or even include corrections to the ES parameters on the basis of experimental observations.

A wide variety of chemical groups can be used as molecular building blocks to construct conjugated systems.[4−6,8,17] Therefore, exhaustive search of molecular structures with desirable electronic and optical properties is time-consuming. The ES approach enables efficient computation of the excited state properties of any molecule formed by any combination of molecular building blocks from the library. Thus, the ES approach can provide a low-cost analysis of the structures, initially constructed by chemical intuition, before the real expensive synthesis and characterization take place.

In the synthesized PA-based molecules,[5,7,8,25] one can find only a short list of molecular vertices (see Figure 1; vertices a, b, and c have been studied within the ES approach). Naturally, one direction of our work is to characterize the remaining PA joints. In this paper, we study two vertices with high degree of symmetry: the triple and quadruple joints shown in Figure 1d and g. The triple joint is a common building block of dendrimeric stars (nanostars).[7] In addition, complex molecular networks[1,2,6,11] can be formed by combining previously characterized vertices with these two joints.

III. RETRIEVING THE SCATTERING MATRICES FOR Y AND X JOINTS

In this section, we describe how the scattering matrices $\Gamma_Y(\omega)$ and $\Gamma_X(\omega)$ for the triple Y and quadruple X joints, respectively, can be retrieved using quantum-chemical computations in molecules of moderate sizes. The scattering matrices, associated with the triple and quadruple joints, have dimensions 3×3 and 4×4, respectively. Fortunately, we can take advantage of the high degree of symmetry of these joints (it is a reason why they are referred to as symmetric joints) to simplify the matrix

parametrization. As shown below, due to their symmetry, the symmetric molecules can be viewed as effective linear chains, and the same computational procedure as for linear and two-arm molecules[41,43,46] can be employed to extract the scattering matrix elements.

A. Symmetry Analysis. The scattering matrix $\Gamma(\omega)$, associated with a degree-n vertex represents a unitary linear transformation from the space $V^{(-)}$ of incoming to the space $V^{(+)}$ of outgoing waves at frequency ω, the latter standing for the excitation energy. Generally, planar vertices can remain invariant with respect to certain rotations and reflections that generate the vertex symmetry group G. Elements $g \in G$ of the symmetry group are naturally represented in the spaces $V^{(\pm)}$ by unitary operators $T(g)$, so that they act in the space of scattering matrices as $\Gamma \rightarrow T(g)^{-1} \Gamma T(g)$. In the following, we will use group representation theory[50] to parametrize the scattering matrices.

We start with the symmetric Y joint. Its symmetry group $G_Y = D_3$ (a dihedral nonabelian group with six elements including the rotations by $\pm 2\pi/3$ and three reflections) determines a form of the associated scattering matrix

$$\Gamma_Y(\omega) = \begin{pmatrix} r & t & t \\ t & r & t \\ t & t & r \end{pmatrix} \qquad (4)$$

with $r(\omega)$ and $t(\omega)$ being complex numbers that represent the reflection and transmission amplitudes, respectively. The unitarity of the scattering matrix Γ_Y imposes two independent (real) conditions on r and t, allowing Γ_Y to be parametrized by two real parameters. Indeed, the group D_3 has two irreducible representations: a one-dimensional trivial representation and a two-dimensional representation. The former corresponds to the symmetric incoming and outgoing waves, or in other words, the zero angular momentum, $m = 0$. The space of the second representation is spanned by two angular harmonics with $m = \pm 1$, interchanged by reflections. Therefore, the matrix Γ_Y can be diagonalized in an ω-independent basis:

$$\Gamma_Y = UDU^\dagger \qquad (5)$$

$$U = \frac{1}{\sqrt{3}} \begin{pmatrix} 1 & 1 & 1 \\ 1 & \exp(2\pi i/3) & \exp(-2\pi i/3) \\ 1 & \exp(-2\pi i/3) & \exp(2\pi i/3) \end{pmatrix}$$

$$D = \begin{pmatrix} \exp(i\phi_S) & 0 & 0 \\ 0 & \exp(i\phi_P) & 0 \\ 0 & 0 & \exp(i\phi_P) \end{pmatrix}$$

In each representation, the scattering matrix acts as a reflection amplitude with the unit absolute value. Therefore, $\Gamma_Y(\omega)$ is parametrized by only two real energy-dependent scattering phases, $\phi_S(\omega)$ and $\phi_P(\omega)$. As follows from eq 4, the matrix elements of Γ_Y are related to the scattering phases by

$$\begin{aligned} r &= \frac{1}{3}\left(\exp(i\phi_S) + 2\exp(i\phi_P)\right) \\ t &= \frac{1}{3}\left(\exp(i\phi_S) - \exp(i\phi_P)\right) \end{aligned} \qquad (6)$$

The symmetry group of the X joint is the abelian group $G_X = D_2 \cong \mathbb{Z}_2 \oplus \mathbb{Z}_2$ of order four generated by two reflections
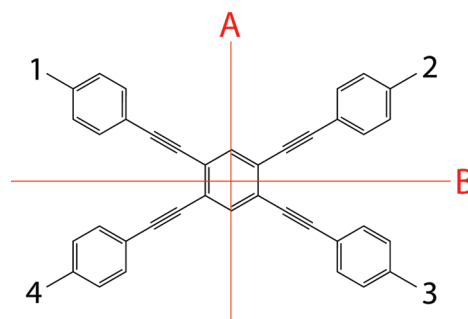
Figure 2. The symmetric quadruple joint (X joint). The arm order (1, 2, 3, 4) and the symmetry axes (A and B) are defined.

(symmetry axes A and B in Figure 2) which has four one-dimensional irreducible representations. Therefore, the 4×4 scattering matrix Γ_X of the X joint can be parametrized by four real phases ϕ_{ab}, corresponding to four symmetries $A^a B^b$ where a and b can assume values 0 and 1 for the symmetric and antisymmetric configurations, or equivalently even and odd parity, respectively. Thus, the matrix $\Gamma_X(\omega)$ can be also diagonalized in an ω-independent basis:

$$\Gamma_X = UDU^\dagger \qquad (7)$$

$$U = \frac{1}{2} \begin{pmatrix} 1 & 1 & 1 & 1 \\ 1 & 1 & -1 & -1 \\ 1 & -1 & -1 & 1 \\ 1 & -1 & 1 & -1 \end{pmatrix}$$

$$D = \begin{pmatrix} \exp(i\phi_{00}) & 0 & 0 & 0 \\ 0 & \exp(i\phi_{01}) & 0 & 0 \\ 0 & 0 & \exp(i\phi_{10}) & 0 \\ 0 & 0 & 0 & \exp(i\phi_{11}) \end{pmatrix}$$

Similar to the symmetric triple joint, each energy-dependent scattering phase represents the reflection phase of an effective terminus that fully describes the X joint for excitations of a particular symmetry. The four scattering phases $\phi_{ab}(\omega)$ are generally different without additional symmetries.

B. Numerical Procedure. The numerical procedure for retrieving the scattering phases of the symmetric triple and quadruple joints from quantum-chemical computations is substantially simplified if we consider only symmetric (equal-arm) molecules with a Y or X joint, that is, the molecules that preserve the symmetry of the corresponding joint. In such molecules, the excited states can be classified according to the irreducible representations of the vertex symmetry groups G_Y and G_X, respectively. In other words, the incoming and outgoing wave amplitudes form eigenvectors of the scattering matrices.

The parametrizations of the scattering matrices, presented above (eqs 5 and 7), suggest the following approach to obtain the scattering phases. For a symmetric molecule with the arms of identical length L, we compute all excitation energies and transition density matrices for a given exciton type. For a certain symmetry of the excited state (determined from its transition density matrix), the scattering at the symmetric joint is equivalent to the terminal scattering for the corresponding effective linear-segment model. Consequently, the value of the corresponding scattering phase $\phi(\omega)$ (which is any of the phases ϕ_S, ϕ_P, ϕ_{00},

ϕ_{01}, ϕ_{10}, and ϕ_{11}) at the excitation energy ω can be found from the quantization relation

$$\phi = 2\pi n - 2kL - \phi_T \qquad (8)$$

where n is an integer, whereas the values of the wavenumber k and the phase ϕ_T of the chain terminus are found from the functions $k = k(\omega)$ and $\phi_T = \phi_T(\omega)$ tabulated previously. In principle, one can use a dense electronic spectrum of only one sufficiently large molecule to determine all features of all energy-dependent scattering phases of the Y or X joint. However, in the CEO computations, where the numerical cost to find all $O(N)$ excitons in the band grows as $O(N^4)$ with the number of electrons N in the molecule, the cost per a single excitation grows as $O(N^3)$. Thus, using several smaller molecules usually leads to a more efficient extraction of the ES parameters, which remains sufficiently accurate as long as the linear segments are long enough to avoid nonlocal influence of the molecular vertices. In addition, using several molecular sizes to obtain the scattering phases gives us an idea about the extent and strength of these nonlocal effects.

We used symmetric Y and X molecules with the arm lengths from 5 to 13 and from 4 to 13 repeat units, respectively. First, we optimized the ground state geometries at the AM1 level in Gaussian03 package.[49] Then for each molecule, we applied the collective electronic oscillator method,[33,34] based on the time-dependent Hartree–Fock (TDHF) theory combined with the semiempirical INDO/S (intermediate neglect of differential overlap parametrized for spectroscopy) Hamiltonian,[51] to compute the vertical transition energies, transition dipoles, and transition density matrices for the first 40 excitations. By checking the transition density matrices, we selected the lowest-energy exciton band;[43] the excitations were further divided into the sets according to their symmetries. Finally, each scattering phase was calculated by using eq 8.

The QC reference method should adequately describe exciton properties, including the binding energy and the exciton size; the latter determines how accurately the ES approach is expected to work in molecules with shorter linear segments. The aforementioned exciton properties strongly depend on the amount of the Hartree–Fock orbital exchange in the density functional.[52,53] For example, TDDFT based on the B3LYP functional with 20% of orbital exchange results in a way too large exciton size and small binding energy; moreover, it is prone to the charge transfer problem.[54] Consequently, it is preferable to use a functional with a medium amount of HF exchange (e.g., BHandH with 50% of orbital exchange) or an asymptotically corrected functional (e.g., CAM-B3LYP or LC functionals). On the other hand, although the TDHF method based on an ab initio basis set tends to overbind the excitons, resulting in a smaller exciton size, the TDHF or CIS approaches based on the semiempirical methods can accurately reproduce the excitonic properties in conjugated polymers (see ref 55 for a detailed analysis). Therefore, we have good reasons to believe that our reference QC based on the semiempirical CEO method is adequate for our applications.

C. Frequency Dependence of the Scattering Phases. The scattering phases of the Y and X joints are shown in Figures 3 and 4 as functions of energy. The two scattering phases of the Y joint are similar to the phases of the meta joint (see Figure 5). These similarities have intuitive interpretation in terms of well-known trends in organic chemistry: meta conjugation at phenyl rings forms a serious obstacle for charge transfer, whereas charge is easily transferred through the ortho and para connections.
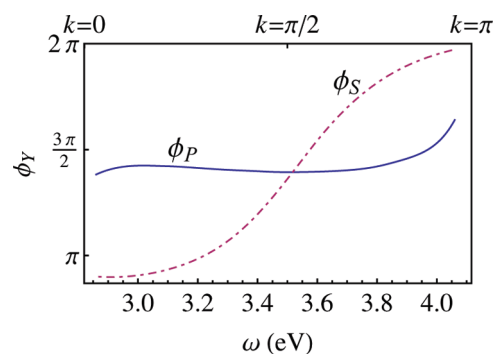
Figure 3. The scattering phases of the Y joint.
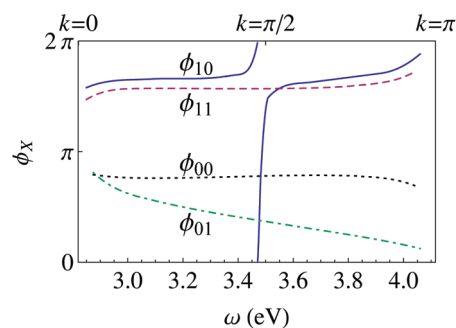
Figure 4. The scattering phases of the X joint. For higher energies, ϕ_{10} is shifted by -2π.
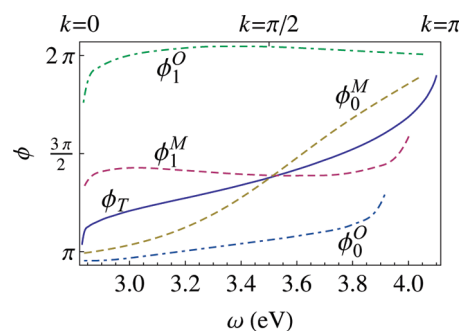
Figure 5. The scattering phases of the meta (M) and ortho (O) joints and the terminus. The scattering phases $\phi_{0,1}^M$ and $\phi_{0,1}^O$ of the double joints are defined according to the irreducible representations of $D_1 \cong \mathbb{Z}_2$, similarly to the phases of the X joint in Section IIIA.

The described property has clear signatures in chemical reactivity. It was argued in the context of experimentally obtained optical spectra in phenylacetylene dendrimers[7] that the above charge transfer properties can be extended to interpret optical properties of branched conjugated molecules. It was later shown theoretically[36] that optical excitations in branched molecules do not involve charge transfer through meta connections and can be coupled only via the coherent energy transfer mechanism. Within the ES approach, scattering at the joints that involve meta conjugation only is attributed to effects of direct Coulomb interaction between the photoinduced charge densities on the connected segments.[40,43] Therefore, the scattering phases that describe the double meta joint and the triple Y joint, both containing meta connections only, show similar frequency dependence for the corresponding symmetries.
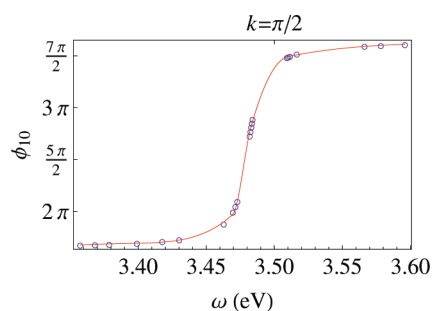
Figure 6. Phase ϕ_{10} of the X joint in the vicinity of the kink. Data points used for fitting are shown together with the fitting curve.
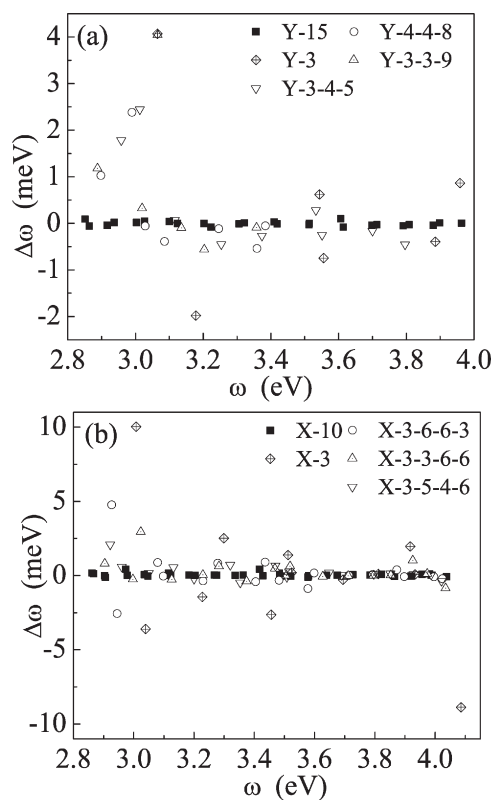
Figure 7. Differences between excitation energies obtained by the ES approach and the CEO technique for selected (a) Y and (b) X molecules. Y-a represents a symmetric Y molecule with the arm length of a repeat units. Y-a-b-c represents an asymmetric Y molecule with the arm lengths of a, b, and c repeat units. Similar notations are used for X molecules with the order of the arms shown in Figure 2.

The behavior of the scattering phases of the X joint, which has all three connections—ortho, meta, and para—is different from that of the Y joint. In particular, we observe a resonance-type behavior for one of the scattering phases (corresponding the symmetry A^1B^0) in the form of an almost-2π kink. As shown in Figure 6, the feature cannot be dismissed as resulting from the outlying points, since several molecules of different sizes contribute to the resonance shape in the phase. The other two phases associated with the X joint also possess a remarkable property: ϕ_{00} and ϕ_{01} seem to decrease by 2π when k changes across the Brillouin zone. All these features will be
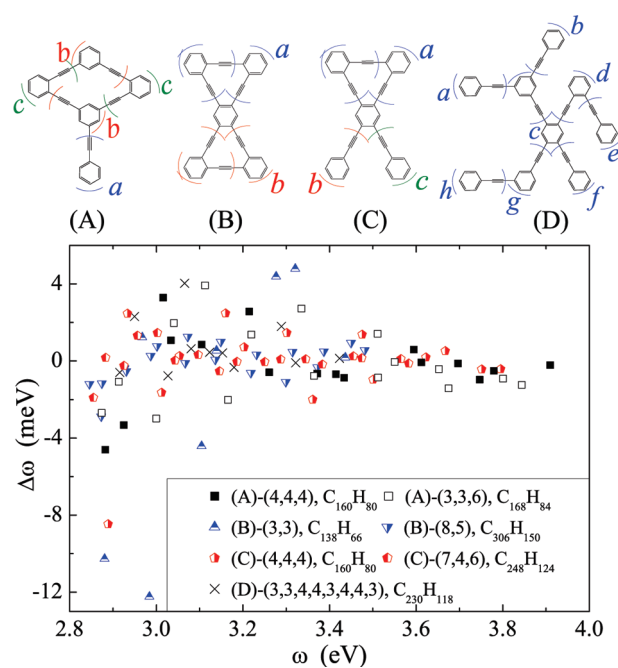
Figure 8. Differences between excitation energies obtained by the ES approach and the CEO technique for selected molecules whose structures are shown in the upper panel. The linear segment lengths and chemical formulas are specified in the legend.

analyzed in Section VB in terms of the topological properties of the scattering phases.

IV. TESTING THE ES APPROACH

Following ref 44, we evaluate the accuracy of the retrieved scattering phases by applying the ES approach to several test molecules with the Y and X joints and comparing the results with the quantum chemistry computations for the corresponding test molecules using the same reference quantum chemistry method (in this study, CEO) as was used for obtaining the ES parameters. The comparison of the transition energies (Figure 7) shows that the energy deviations are usually within 10 meV. We expect the ES approach to be asymptotically exact when the linear segments become much longer than the exciton size. In practice, we usually get good agreement with quantum-chemical transition energies if the segment lengths just exceed the exciton size (which is only 1−2 repeat units). For the molecules tested here, we also observe a quick decrease in the transition energy deviations with increasing segment lengths.

We further extend our test to more complex molecules that include various combinations of meta, ortho, Y, and X joints. The structures that we have considered as well as the results for the deviations are shown in Figures 8 and 9.

Computations for some of these test molecules already push the abilities of even the CEO method (which is relatively numerically inexpensive in comparison with other quantum-mechanical methods) to the limit. As all the results show, the agreement between the ES approach and the reference quantum-chemical computations is quite impressive, and the deviations are similar to those for simpler test molecules.

The combination of molecular building blocks (e.g., as in Figure 9) allows one to build a variety of 2D networks, whose excited state electronic structure can also be efficiently studied using the ES approach.

5470

dx.doi.org/10.1021/jp110317d |*J. Phys. Chem. B* 2011, 115, 5465–5475
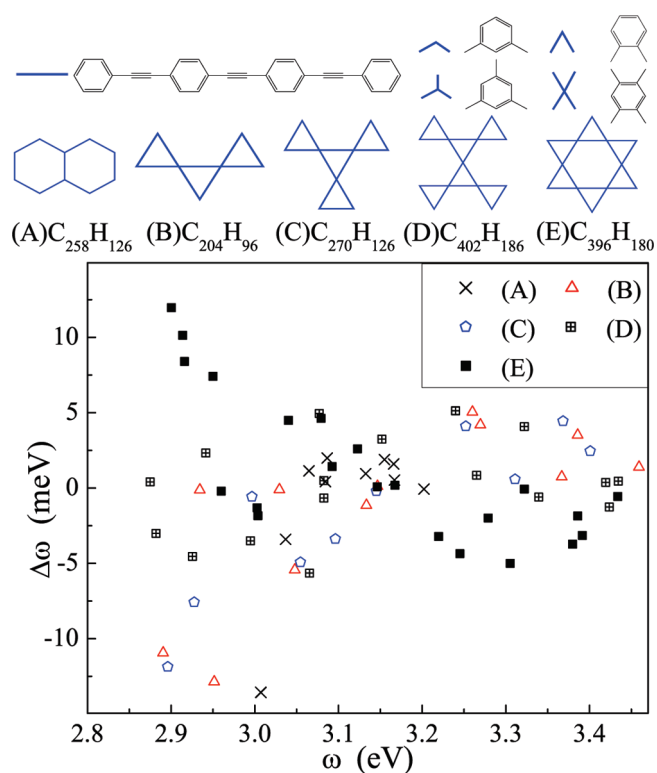
Figure 9. Differences between excitation energies obtained by the ES approach and the CEO technique for some molecules, which can be units of 2D networks (molecular structures are shown in the upper panel; all linear segments have a length of three repeat units).

V. TOPOLOGICAL PROPERTIES OF SCATTERING PHASES AND THEIR PHYSICAL INTERPRETATION

As mentioned in Section IIIC, the frequency dependence of the phases parametrizing the scattering matrix $\Gamma_X(\omega)$ of the X joint has very interesting qualitative features that are unlike the behavior of the phases of all other studied PA vertices. In this section, we present an initial analysis of the analytical properties of the scattering matrices describing symmetric joints, identify simple topological invariants associated with the frequency dependence of the corresponding phases, and determine the physical meaning of the aforementioned qualitative features in terms of the invariants.

A. Analytical Properties of the Scattering Phases and Topological Invariants. This subsection has two goals: (i) introduce a set of integer-valued topological invariants, referred to as the *scattering degrees* of a vertex (one per each independent scattering phase) for a symmetric branching center and (ii) relate the scattering degrees to the total number of excitations in a given exciton band in a molecule that consists of the symmetric branching center attached linear backbone segments of the same length.

We start with analyzing the analytical properties of the scattering matrices $\Gamma(\omega)$ that describe symmetric joints in terms of the topological invariants of the corresponding phases.

As discussed in Section IIIA, scattering at the symmetric vertices is factorized according to irreducible representations of the corresponding symmetry groups. Each phase can be interpreted as the reflection phase at a terminus of some effective linear chain, and thus, the scattering matrix can be efficiently analyzed in these much simpler terms.

The reflection amplitude $r(\omega) = e^{i\phi(\omega)}$ at a terminus of a linear chain is defined as the ratio of the outgoing and incoming waves amplitudes. To identify the topological properties of the scattering amplitude, we will consider it as a function, $r(k)$, of the exciton momentum, related to the frequency via the exciton spectrum $\omega = \omega(k)$, rather than the frequency itself. Within the ES picture, the wave function of an exciton, with the energy $\omega = \omega(k) = \omega(-k)$, on a finite segment or semi-infinite linear chain, is a superposition of two plane waves with the momenta $\pm k$,

$$\psi(y) = e^{-ik(y-x)} + r_x(k)\, e^{ik(y-x)} \qquad (9)$$

where y is an integer coordinate of a repeat unit, and x is a reference point that can be chosen arbitrarily. Note that due to the time-reversal symmetry of all systems under consideration, in addition to $\omega(k) = \omega(-k)$, eq 9 implies $r(-k) = r^{-1}(k)$. Naturally, the reflection phase depends in a prescribed way on a particular choice of the reference point, x:

$$r_x(k) = r_0(k)\, e^{2ikx} \qquad (10)$$

and if the reference point x is chosen, the scattering phase is well-defined. Therefore, a notation $r(k)$ means that the reference point is fixed in some way.

To identify a relevant topological invariant, we start with noting that, since the translational symmetry of our problem is discrete, that is, $y, x \in \mathbb{Z}$ in eqs 9 and 10, the exciton momentum (strictly speaking, quasimomentum) is defined in a 1D Brillouin zone, say, $0 \le k \le 2\pi$, with the points $k = 0$ and $k = 2\pi$ being equivalent. Therefore, introducing a new variable $z = e^{ik}$ makes sense, and the quasimomentum can be treated as residing in a unit circle $|z| = 1$ in a complex plain $\mathbb{C}$. By its definition, the scattering amplitude $r = e^{i\phi}$ also resides in a unit circle $|r| = 1$ of the complex plain.

Therefore, the scattering phase, as a function $\phi(\omega)$ of the exciton frequency, or equivalently, as a function $\phi(k)$ of the exciton momentum, can be viewed as $r(z)$, that is, a map $S^1 \to S^1$ of a circle $|z| = 1$ to a circle $|r| = 1$. Such a map has a simple and very natural integer topological invariant $m \in \mathbb{Z}$, referred to as the *degree* of the map,[56] that represents the number of times $r(z) = e^{i\phi(k)}$ winds over the circle, while $z = e^{ik}$ goes once over the Brillouin zone. This winding number can be represented as

$$m = \int_0^{2\pi} \frac{dk}{2\pi} \frac{d\phi(k)}{dk} \qquad (11)$$

$$= \oint_{|z|=1} \frac{dz}{2\pi i}\, r^{-1}(z)\, \frac{dr(z)}{dz} \qquad (12)$$

Summarizing, we have associated with any terminus a topological invariant m_x, referred to as the *degree of the terminus* (or the corresponding scattering phase), defined by eq 12 in terms of the scattering amplitude $r_x(z)$, which depends in a prescribed way on a particular choice of the reference point (i.e., m_x changes by 2 when x changes by 1). Note that due to the latter property (which immediately follows from eq 10), the position of the reference point x, which was initially restricted to integer values, can be extended also to half-integers if the latter choice makes the formalism more convenient.

The half-integer choice of x turns out to be convenient for the considered case of PA oligomers: we define the scattering amplitude at positions $x = 1/2$ on the linear segments (shifted by $-1/2$ from the first repeat unit of the segment, when counted from the vertex) to obtain a simple relation between the outgoing
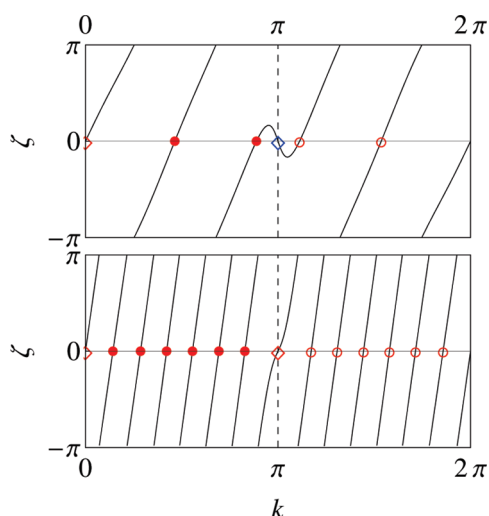
Figure 10. Graphical solution of eq 13 is represented as finding intersections of two closed curves on the torus. The fundamental polygons of the torus are shown for the A^0B^0 states in symmetric X molecules with arm lengths of two (top) and seven (bottom) repeat units. Circles and diamonds denote formal solutions (intersections): physical solutions in the first Brillouin half-zone (filled circles), their counterparts in the second half-zone (open circles), and unphysical solutions $k = 0$ and $k = \pi$ (diamonds). The symbols are red and blue for positive and negative individual intersection indices, respectively. The number of states in the band is represented by the number of filled circles.

wave on one end of the segment and the incoming wave on its other end (eq 2), which leads to a quantization condition in the form of eq 8.

Having introduced the scattering degrees associated with the relevant vertices, which accomplishes goal i, we are now in a position to achieve the goal ii, described at the very beginning of this subsection. To that end, we start with noting that in a linear segment with the length L (measured in repeat units) with two termini A and B described by the reflection phases $\phi_A(k)$ and $\phi_B(k)$, the quantization condition

$$2kL + \phi_A(k) + \phi_B(k) = 2\pi q \tag{13}$$

is satisfied with an integer q for a state that consists of two plane waves with the wavenumbers $\pm k$. Therefore, the solutions of eq 13 that are labeled by the opposite values of k correspond to the same physical state, and counting the solutions of eq 13, we count each physical state twice.

To count the solutions of eq 13, we consider a torus $T^2 = S^1 \times S^1$ that consists of the points (k, ζ) [or, to be more precise, of $(e^{ik}, e^{i\zeta})$] and note that a solution of eq 13 can be represented as an intersection point on the torus T^2 of the closed curve C defined by the equation

$$\zeta = 2kL + \phi_A(k) + \phi_B(k) \tag{14}$$

with a simple circular curve C_0 defined by $\zeta = 0$ (an illustration is given in Figure 10 in the next subsection). We also note that, since the scattering phases satisfy the conditions $\phi(0) = \pi$ and $\phi(\pi) = 0$, there are two solutions (intersections) with $k = 0$ and $k = \pi$, respectively, which do not correspond to physical excited states, being represented by zero wave functions.

The reason for relating the number of excited states to the number of intersection points of two curves on a torus is to apply the concept of *intersection index*,[56] denoted by $C*C_0$. If the curves

intersect transversally (i.e., their tangent vectors at any intersection point are linearly independent), the intersection index is given by

$$C*C_0 = \sum_{x \in C \cap C_0} \text{ind}_x \tag{15}$$

where the intersection index $\text{ind}_x = \pm 1$ of an individual intersection point is determined by the relative orientation of the tangent vectors of the curves at the considered intersection point and in our case is given by

$$\text{ind}_{(k, \zeta)} = \text{sign}(d\zeta(k)/dk) \tag{16}$$

where $\zeta(k)$ is given by eq 14.

The intersection index can be used to count the number of intersections of two curves by utilizing its property of being a topological invariant: $C*C_0$ is invariant with respect to continuous deformations of the curves and is explicitly expressed in terms of the topological invariants of the latter.[56] More specifically, we have

$$C*C_0 = n_2(C)\, n_1(C_0) - n_2(C_0)\, n_1(C) \tag{17}$$

where for any curve, C, on the torus, $n_1(C)$ and $n_2(C)$ denote how many times the curve winds along the first and second cyclic coordinates on the torus, k and ζ, respectively. For our particular choice of the curves, we have $n_1(C_0) = 1$, $n_2(C_0) = 0$, $n_1(C) = 1$, and $n_2(C) = 2L + m_A + m_B$. The first three equalities are obvious, and the last is obtained by calculating a winding number of $\zeta(k)$ similarly to eq 11. This results in

$$C*C_0 = \sum_{x \in C \cap C_0} \text{ind}_x = 2L + m_A + m_B \tag{18}$$

Recalling our earlier statement on the relation between the number of physical states N in the band to the total number of (unsigned) intersections between C and C_0, we have

$$N = 1/2 \sum_{x \in C \cap C_0} |\text{ind}_x| - 1 \tag{19}$$

where, in particular, one unphysical state (that corresponds to two unphysical intersections) is subtracted.

In a general situation, the relation between the intersection index and the total number of intersection points is complex. When the curves are deformed, the intersections can appear and disappear, changing the total number of intersection points. However, the intersection index remains unchanged, since the transverse intersections appear and disappear in pairs with opposite individual intersection indices. Stated differently, the intersection index, being a topological invariant, is easy to compute, whereas we are actually interested in the total number of intersections.

The situation becomes simple when all individual intersection indices ind_x have the same value. This happens for a sufficiently long linear segment, when $d\zeta(k)/dk > 0$ for all k, and eqs 19 and 18 result in a general relation

$$N = L + Q_A + Q_B \tag{20}$$

that expresses the total number N of excitations in an exciton band in terms of the number L of repeat units between the termini and the topological charges Q_A and Q_B of the reflection phases, with a topological charge $Q = (m-1)/2$ being explicitly expressed in terms of the scattering degree.

Note that eq 20 should and does hold, regardless of particular choices of the reference points x that affect the reflection amplitudes, according to eq 10. Indeed, a shift of the reference point x by 1 repeat unit changes the corresponding scattering degree m by 2, which results in the change of the topological charge Q by 1; the latter is compensated in eq 20 by the corresponding change of the number L of repeat units by -1. Stated differently, the definition of the scattering phase is consistent with the corresponding agreement on the number of repeat units. Typically, with our definition of the reference point for the reflection phase, the scattering degrees m are odd numbers, so that the corresponding topological charges Q that enter eq 20 are integers.

For most scattering phases that we found in PA oligomers, $Q = 0$, that is, the phase increases by π when k changes from 0 to π, and the number of states in the exciton band is equal to the number of repeat units. This is the case also for the states of certain symmetry in the symmetric molecules with symmetric branching centers. In most cases, we do not observe strong negative slopes of the phase as a function of wavenumber, which means that the number of states should equal the number of repeat units, even in the shortest molecules. Indeed, this is exactly what we observe in quantum-chemical computations in these typical cases.

B. Topological Analysis of the X Joints. At the end of section III we have briefly discussed some interesting features observed in the energy (or, equivalently, wavenumber) dependence of the scattering phases characterizing the X joint (see Figures 4 and 6). In this subsection, we apply the analysis of the number of exciton states inside the band, presented in subsection VA, to draw parallels between the characteristic features of the scattering phases and quantum-chemical results for equal-arm molecules with the X joint. Since, as noted in subsection VA, the time-reversal symmetry implies $\phi(k) = -\phi(-k) = -\phi(2\pi-k)$, any scattering phase is completely described by its behavior on a half of the Brillouin zone, say, at $0 \leq k \leq \pi$.

Although we do not have enough data for the phases of the X joint at the band edges, the overall behavior of the phases ϕ_{10} and ϕ_{01} indicates that they change by 3π and $-\pi$, respectively, over the half of the Brillouin zone. The evidence in the case of the A^0B^0 symmetry is not as clear as for the first two cases. Nevertheless, the behavior of ϕ_{00} suggests that it has $Q = -1$ and a fast decrease near $k = \pi$ (we can expect ϕ_{00} to be equal to 0 at $k = \pi$ due to the observed slope and curvature, although we do not have sufficient data to confirm this property). Finally, the phase ϕ_{11} seems to change by π over the half Brillouin zone; that is, by the same amount as all phases of the other studied PA vertices (see Figures 3 and 5 as well as ref 46), including the reflection phase at the unmodified PA terminus (phenyl ring).

Thus, we find three distinct cases for the scattering phases of the X joint: $Q = 0$ for ϕ_{11}, $Q = 1$ for ϕ_{10}, and $Q = -1$ for ϕ_{01} and ϕ_{00}. The following detailed analysis in the equal-arm X molecules with free ends will also use that the unmodified PA terminus is characterized by $Q = 0$.

For the phase ϕ_{10} with a 2π-kink in each half of the Brillouin zone, we have $Q = 1$, which, according to eq 20, should result in one additional state inside the band. Indeed, the number of A^1B^0 states in quantum-chemical computations in X molecules with the arm length L is equal to $L + 1$. Moreover, the abrupt change of ϕ_{10} implies that the additional state is a resonance at almost the same energy for any arm length, what we actually observe. Correspondingly, in quantum-chemical transition density matrices,

such states look like superpositions of a state localized on the X joint and standing waves with the reduced amplitudes in the arms. The width of the kink in ϕ_{10} can be interpreted as the strength of the coupling between the state on the X joint and the excitations in the linear segments; the small width points to weak coupling. In other words, the kink in the scattering phase is a signature of the peak in the density of states that would be found in the X molecule with semi-infinite arms.

The phase ϕ_{01} is characterized by a relatively uniform negative slope and topological charge $Q = -1$, which, according to the analysis in the previous subsection, implies that for all arm lengths, there is one fewer state of the symmetry A^0B^1 in the exciton band. Indeed, although in quantum chemistry results for X molecules with the identical arm length L, there are L states with the A^0B^1 symmetry, one of them is always bound with its energy below the band. Thus, we see that such a gradual decrease of the scattering phase with $Q = -1$ is associated with the converting of one of the states of the band into a strongly bound state.

For the long enough arm length L, one should have $L - 1$ excitations with the A^0B^0 symmetry inside the band. In the molecules with the arm length $L \leq 5$, quantum chemistry provides L excitations with the A^0B^0 symmetry, and we do not have high-energy results for bigger molecules due to computational limitations. Nevertheless, on the basis of the data obtained from the molecules where quantum-chemical computations are still possible, the resulting trend in the phase ϕ_{00} corresponds to an observation that the last excitation approaches the band edge relatively quickly as the arm length increases. In addition, according to our preliminary results on analytic continuation of the scattering amplitudes to complex values of k, the curvature in the dependence $\phi_{00}(k)$ may correspond to the bound state above the band, in contrast to the shape of $\phi_{01}(k)$, for which the bound state is below the band. Thus, our observations for the A^0B^0 symmetry, although incomplete, do not contradict the general analysis presented in the previous subsection. We expect that in the X molecules with longer arms, one will find a weakly bound state above the band converted from the state in the band. Alternatively, one can say that a state weakly bound at an end of a long segment enters the band when the segment becomes so short that the scattering at its other end sufficiently changes the state energy.

In Figure 10 we illustrate an application of the analysis of subsection VA to A^0B^0 states in symmetric X molecules: we first interpolate $\phi_{00}(k)$ and the reflection phase $\phi_T(k)$ of the terminus in the whole Brillouin zone and then show the closed curve $\{(k, \zeta)|\zeta = \zeta(k)\}$ (see eq 14) in the fundamental polygon (in this case, a square) $\{(k, \zeta)|k \in [0, 2\pi), \zeta \in [-\pi, \pi)\}$ of the torus. Solutions of $\zeta(k) = 2\pi q$ (eq 13) are shown as intersections on the torus for two molecules with different arm lengths. The degrees of the scattering phases involved (ϕ_T and ϕ_{00}) are $m_T = 1$ and $m_{00} = -1$, respectively. Therefore, according to eq 18, the total intersection index should be $C*C_0 = 2L$ for the symmetric X molecules with the arms of length L. In the molecule with $L = 2$, the upper panel of Figure 10 shows two A^0B^0 states in the band (since the solution $k = \pi$ has a negative intersection index, the total number of solutions in the Brillouin zone is $C*C_0 + 2 = 6$, of which 2 are unphysical, which yields $(6 - 2)/2 = 2$ states in the band). In the molecule with $L = 7$, the lower panel of Figure 10 shows six A^0B^0 states in the band ($L = 7$ is big enough for all solutions to have positive intersection indices, and the total

5473

dx.doi.org/10.1021/jp110317d |*J. Phys. Chem. B* 2011, 115, 5465–5475

number of solutions in the Brillouin zone is $C*C_0 = 14$, of which 2 are unphysical, which yields $(14 - 2)/2 = 6$ states in the band).

In conclusion, in relatively small symmetric molecules with the X joint, we observe that it binds one A^0B^1 state from the exciton band and introduces an additional A^1B^0 state inside the band. In fact, for energies below and above the kink in ϕ_{10}, the excitations of different symmetries appear in the order determined by the decreasing phase values at a given energy (A^1B^0, A^1B^1, A^0B^0, A^0B^1, A^1B^0, ...; see Figure 4), while the inserted A^0B^1 state violates the order in the region of the kink. Thus, the available data on the number of states and their symmetries, obtained via quantum chemistry computations for symmetric X molecules, are in complete agreement with the analysis presented in the previous subsection. Similar comparison for other vertices, which all have $Q = 0$, also confirms the relation 20; those simpler situations are not discussed here.

VI. CONCLUSIONS

In this paper, we report our results on the further developments of the exciton scattering (ES) approach, designed for efficient calculations of electronic excitations in branched conjugated molecules. First, we considered exciton scattering properties of the symmetric triple and quadruple joints, referred to as Y and X joints, respectively. We characterized them with the scattering matrices according to their symmetries and retrieved the relevant phases parametrizing the matrices from quantum chemistry calculations. We compared the results of the ES approach with the results of complete computations using the reference quantum-mechanical method in several test molecules, including the newly characterized vertices, and found excellent quantitative agreement for transition energies. Next, we presented an initial analysis of the relations between the number of the exciton states in the band, the number of repeat units, and characteristic features of the scattering phases as functions of the wavenumber. We observed that the phases of the X joint corresponding to different symmetries exhibit different types of behavior and found that their features are in agreement with the quantum-mechanical results for symmetric X molecules. These results provide another demonstration of the usefulness of the ES approach for understanding electronic excitations in conjugated molecules.

We conclude with indicating several directions of our future research with the ultimate goal of developing an efficient computational approach for description and analysis of electronic and optical properties of large branched conjugated molecules. We are following the way common in condensed matter physics: first, we identify and characterize free noninteracting particle-like excitations (excitons) and, later, intend to characterize their interactions with phonons and static disorder. This will allow us to build efficient approaches for treating not only light absorption but also photoinduced dynamics, including energy transfer and finite lifetimes of the excitons due to their dissipation or recombination, in realistic imperfect oligomers.

As a way to actualize this program, we have to reduce the number of parameters used for description of electronic excitation and study their dependence on the geometrical distortions. We already observed[41,43] that the exciton dispersion $\omega(k)$, extracted from the quantum-chemical computations, can be adequately approximated by a small number of cosine harmonics, which is exactly the form one finds in tight-binding lattice models with possible hopping between close neighbors.

We have reasons to believe that the frequency/wavenumber dependence of the scattering matrices can also be represented by a few lattice model parameters. Thus, instead of high-dimensional parametrization of the full ES approach (which involves fitting functions on several intervals), we will deal with a reasonably small number of meaningful parameters, associated with the effective exciton lattice model, that will be obtained from the reference quantum-chemical method via the ES methodology. In addition, analytical expressions for the scattering matrices derived within a lattice model can be used for analytic continuation, which will allow us, in particular, to deduce the positions of possible bound states from the scattering phases. Thus, the analysis of analytical and topological properties of the scattering matrices initiated in this work will be completed with the help of the lattice-model description to eventually serve as an important criterion for choosing an appropriate lattice model.

■ AUTHOR INFORMATION

Corresponding Author

*E-mails: chernyak@chem.wayne.edu (V.Y.C.); serg@lanl.gov (S.T.).

■ REFERENCES

(1) Baughman, R. H.; Eckhardt, H.; Kertesz, M. *J. Chem. Phys.* **1987,** *87,* 6687–6699.

(2) Diederich, F. *Nature* **1994,** *369,* 199–207.

(3) Devadoss, C.; Bharathi, P.; Moore, J. S. *J. Am. Chem. Soc.* **1996,** *118,* 9635–9644.

(4) Bunz, U. H. F. *Adv. Polym. Sci.* **2005,** *177,* 1–52.

(5) Zhang, W.; Moore, J. S. *Angew. Chem., Int. Ed.* **2006,** *45,* 4416–4439.

(6) Spitler, E. L.; Johnson, C. A.; Haley, M. M. *Chem. Rev.* **2006,** *106,* 5344–5386.

(7) Kopelman, R.; Shortreed, M.; Shi, Z. Y.; Tan, W. H.; Xu, Z. F.; Moore, J. S.; Bar-Haim, A.; Klafter, J. *Phys. Rev. Lett.* **1997,** *78,* 1239–1242.

(8) Peng, Z. H.; Melinger, J. S.; Kleiman, V. *Photosynth. Res.* **2006,** *87,* 115–131.

(9) Goodson, T. G. *Acc. Chem. Res.* **2005,** *38,* 99–107.

(10) Barbara, P. F.; Gesquiere, A. J.; Park, S. J.; Lee, Y. J. *Acc. Chem. Res.* **2005,** *38,* 602–610.

(11) Bhaskar, A.; Ramakrishna, G.; Haley, M. M.; Goodson, T. *J. Am. Chem. Soc.* **2006,** *128,* 13972–13973.

(12) Fréchet, J. M. J. *Science* **1994,** *263,* 1710–1715.

(13) Moser, J. E.; Bonnote, P.; Gratzel, M. *Coord. Chem. Rev.* **1998,** *171,* 245–250.

(14) Gust, D.; Moore, T. A.; Moore, A. L. *Acc. Chem. Res.* **2001,** *34,* 40–48.

(15) Forrest, S. R. *Nature* **2004,** *428,* 911–918.

(16) Gunes, S.; Neugebauer, H.; Sariciftci, N. S. *Chem. Rev.* **2007,** *107,* 1324–1338.

(17) Malliaras, G.; Friend, R. H. *Phys. Today* **2005,** *58,* 53–58.

5474

dx.doi.org/10.1021/jp110317d |*J. Phys. Chem. B* 2011, 115, 5465–5475

(18) Gledhill, S. E.; Scott, B.; Gregg, B. A. *J. Mater. Res.* **2005**, *20*, 3167–3179.

(19) Waldauff, C.; Schilinsky, P.; Hauch, J.; Brabec, C. J. *Thin Solid Films* **2004**, *451−52*, 503–507.

(20) Kamat, P. V. *J. Phys. Chem. C* **2007**, *111*, 2834–2860.

(21) Service, R. F. *Science* **2005**, *310*, 1762–1763.

(22) Brédas, J. L.; Cornil, J.; Beljonne, D.; dos Santos, D. A.; Shuai, Z. *Acc. Chem. Res.* **1999**, *32*, 267–276.

(23) Moses, D.; Wang, J.; Heeger, A. J.; Kirova, N.; Brazovski, S. *Proc. Natl. Acad. Sci., U.S.A.* **2001**, *98*, 13496–13500.

(24) Dreuw, A.; Head-Gordon, M. *Chem. Rev.* **2005**, *105*, 4009–4037.

(25) Ortiz, W.; Krueger, B. P.; Kleiman, V. D.; Krause, J. L.; Roitberg, A. E. *J. Phys. Chem. B* **2005**, *109*, 11512–11519.

(26) Scholes, G. D.; Rumbles, G. *Nat. Mater.* **2006**, *5*, 683–696.

(27) Varnavski, O.; Yan, X.; Mongin, O.; Blanchard-Desce, M.; Goodson, T. *J. Phys. Chem. C* **2007**, *111*, 149–162.

(28) Scholes, G. D. *ACS Nano* **2008**, *2*, 523–537.

(29) Heijs, D. J.; Malyshev, V. A; Knoester, J. *Phys. Rev. Lett.* **2005**, *95*, 177402.

(30) Liu, L. T.; Yaron, D.; Sluch, M. I.; Berg, M. A. *J. Phys. Chem. B* **2006**, *110*, 18844–18852.

(31) Dykstra, T. E.; Hennebicq, E.; Beljonne, D.; Gierschner, J.; Claudio, G.; Bittner, E. R.; Knoester, J.; Scholes, G. D. *J. Phys. Chem. B* **2009**, *113*, 656–667.

(32) Tretiak, S.; Chernyak, V.; Mukamel, S. *Chem. Phys. Lett.* **1996**, *259*, 55–61.

(33) Mukamel, S.; Tretiak, S.; Wagersreiter, T.; Chernyak, V. *Science* **1997**, *277*, 781–787.

(34) Tretiak, S.; Mukamel, S. *Chem. Rev.* **2002**, *102*, 3171–3212.

(35) Tretiak, S.; Chernyak, V.; Mukamel, S. *Chem. Phys. Lett.* **1998**, *287*, 75–82.

(36) Tretiak, S.; Chernyak, V.; Mukamel, S. *J. Phys. Chem. B* **1998**, *102*, 3310–3315.

(37) Chernyak, V.; Volkov, S. N.; Mukamel, S. *Phys. Rev. Lett.* **2001**, *86*, 995–99.

(38) Chernyak, V.; Volkov, S. N.; Mukamel, S. *J. Phys. Chem. A* **2001**, *105*, 1988–2004.

(39) Tretiak, S.; Saxena, A.; Martin, R. L.; Bishop, A. R. *J. Phys. Chem. B* **2000**, *104*, 7029–7037.

(40) Wu, C.; Malinin, S. V.; Tretiak, S.; Chernyak, V. Y. *Nat. Phys.* **2006**, *2*, 631–638.

(41) Wu, C.; Malinin, S. V.; Tretiak, S.; Chernyak, V. Y. *Phys. Rev. Lett.* **2008**, *100*, 057405.

(42) Wu, C.; Malinin, S. V.; Tretiak, S.; Chernyak, V. Y. *J. Chem. Phys.* **2008**, *129*, 174111.

(43) Wu, C.; Malinin, S. V.; Tretiak, S.; Chernyak, V. Y. *J. Chem. Phys.* **2008**, *129*, 174112.

(44) Wu, C.; Malinin, S. V.; Tretiak, S.; Chernyak, V. Y. *J. Chem. Phys.* **2008**, *129*, 174113.

(45) Li, H.; Malinin, S. V.; Tretiak, S.; Chernyak, V. Y. *J. Chem. Phys.* **2010**, *132*, 124103.

(46) Li, H.; Wu, C.; Malinin, S. V.; Tretiak, S.; Chernyak, V. Y. *J. Phys. Chem. Lett.* **2010**, *1*, 3396–3400.

(47) Spano, F. C. *Annu. Rev. Phys. Chem.* **2006**, *57*, 217–243.

(48) Brédas, J. L.; Silbey, R. *Science* **2009**, *323*, 348–349.

(49) Frisch, M. J.; Trucks, G. W.; Schlegel, H. B.; Scuseria, G. E.; Robb, M. A.; Cheeseman, J. R.; Montgomery, J. A., Jr.; Vreven, T.; Kudin, K. N.; Burant, J. C.; Millam, J. M.; Iyengar, S. S.; Tomasi, J.; Barone, V.; Mennucci, B.; Cossi, M.; Scalmani, G.; Rega, N.; Petersson, G. A.; Nakatsuji, H.; Hada, M.; Ehara, M.; Toyota, K.; Fukuda, R.; Hasegawa, J.; Ishida, M.; Nakajima, T.; Honda, Y.; Kitao, O.; Nakai, H.; Klene, M.; Li, X.; Knox, J. E.; Hratchian, H. P.; Cross, J. B.; Bakken, V.; Adamo, C.; Jaramillo, J.; Gomperts, R.; Stratmann, R. E.; Yazyev, O.; Austin, A. J.; Cammi, R.; Pomelli, C.; Ochterski, J. W.; Ayala, P. Y.; Morokuma, K.; Voth, G. A.; Salvador, P.; Dannenberg, J. J.; Zakrzewski, V. G.; Dapprich, S.; Daniels, A. D.; Strain, M. C.; Farkas, O.; Malick, D. K.; Rabuck, A. D.; Raghavachari, K.; Foresman, J. B.; Ortiz, J. V.; Cui, Q.; Baboul, A. G.; Clifford, S.; Cioslowski, J.; Stefanov, B. B.; Liu, G.; Liashenko, A.; Piskorz, P.; Komaromi, I.; Martin, R. L.; Fox, D. J.; Keith, T.; Al-Laham, M. A.; Peng, C. Y.; Nanayakkara, A.; Challacombe, M.; Gill, P. M. W.; Johnson, B.; Chen, W.; Wong, M. W.; Gonzalez, C.; Pople, J. A. *Gaussian 03 (Rev. C.02)* Gaussian, Inc.: Wallingford, CT, 2003.

(50) Landau, L. D.; Lifshitz, E. M. *Quantum Mechanics (Non-Relativistic Theory)*; Pergamon Press: Elsmford, NY, 1991, Vol. 3.

(51) Zerner, M. C. *ZINDO: A Semiempirical Quantum Chemistry Program: Quantum Theory Project*; University of Florida, Gainesville, FL, 1996.

(52) Tretiak, S.; Igumenshchev, K.; Chernyak, V. *Phys. Rev. B* **2005**, *71*, 033201.

(53) Igumenshchev, K.; Tretiak, S.; Chernyak, V. *J. Chem. Phys.* **2007**, *127*, 114902.

(54) Magyar, R. J.; Tretiak, S. *J. Chem. Theory Comput.* **2007**, *3*, 976–987.

(55) Moore, E.; Gherman, B.; Yaron, D. *J. Chem. Phys.* **1997**, *106*, 4216–4227.

(56) Hirsch, M. W. *Differential Topology*; Springer: New York, 1997.